

Systematic analysis of doubly charmed baryons Ξ_{cc} and Ω_{cc}

Guo-Liang Yu^{1,*}, Yan Meng¹, Zhen-Yu Li^{2,†}, Zhi-Gang Wang^{1,‡} and Lu Jie¹

¹ *Department of Mathematics and Physics, North China Electric Power University, Baoding 071003, People's Republic of China*

² *School of Physics and Electronic Science, Guizhou Education University, Guiyang 550018, People's Republic of China*

(Dated: July 7, 2023)

In this work, we perform a systematic study of the mass spectra, the root mean square(r.m.s.) radii and the radial density distributions of the doubly charmed baryons Ξ_{cc} and Ω_{cc} . The calculations are carried out in the frame work of relativized quark model, where the baryon is regarded as a three-body system of quarks. Our results show that the excited energy of doubly charmed baryon with ρ -mode is lower than those of the λ -mode and λ - ρ mixing mode, which indicates that the lowest state is dominated by the ρ -mode. According to this conclusion, we systematically investigate the mass spectra, the r.m.s. radii of the ground and excited states($1S \sim 4S$, $1P \sim 4P$, $1D \sim 4D$, $1F \sim 4F$ and $1G \sim 4G$) with ρ -mode. Using the wave functions obtained from quark model, we also study the radial density distributions. Finally, with the predicated mass spectra, the Regge trajectories of Ξ_{cc} and Ω_{cc} in the (J, M^2) plane are constructed, and the slopes, intercepts are determined by linear fitting. It is found that model predicted masses fit nicely to the constructed Regge trajectories.

1. INTRODUCTION

The investigation of doubly heavy baryons is of great interest to experimental and theoretical physicist, as it provides a good opportunity for us to understand the strong interactions and basic QCD theory. Up to now, many single heavy baryons have been well discovered by Belle, BABAR, CLEO and LHCb collaborations[1] and the mass spectra of single heavy baryons have become more and more abundance. However, searching for doubly heavy baryons in experiments ended with no progress for a long time. The first observation of a doubly heavy baryon $\Xi_{cc}^+(3519)$ was reported by the SELEX collaboration in 2002 in the decay mode $\Xi_{cc}^+ \rightarrow \Lambda_c^+ K^- \pi^+$ [2]. Although SELEX collaboration confirmed this state in another decay mode $p D^+ K^-$ [3], the FOCUS, BaBar, Belle and LHCb collaborations reported no evidence of the production of this doubly charmed baryon[4–7]. The breakthrough came in 2017 with the discovery of a doubly charmed baryon Ξ_{cc}^{++} by the LHCb collaboration[8]. This state was observed in the decay mode $\Xi_{cc}^{++} \rightarrow \Lambda_c^+ K^- \pi^+ \pi^+$ with a measured mass $3621.40 \pm 0.72 \pm 0.14 \pm 0.27$ MeV and later was confirmed in another decay mode $\Xi_{cc}^{++} \rightarrow \Lambda_c^+ \pi^+$ [9, 10].

In theory, the mass spectra of the doubly heavy baryons have been predicted with various methods, such as the relativistic or nonrelativistic quark model[11–38], QCD sum rules[39–47], bag models[48–51], the Bethe-Salpeter equation[52–55], effective field theories[56–59], Lattice QCD[60–66] and the others[67–71]. To our knowledge, only Refs.[13, 31] focused on the mass spectra of the doubly heavy baryons from the ground states to the high excited states systematically in the quark-diquark picture. Under this picture, the initial three-body problem is reduced to two-step two-body calculations. However, the popular quark-diquark picture of a baryon is not universal and its results needs further confirmation by different methods. Thus, it is necessary for

us give a systematic analysis of the properties of ground and excited states of doubly heavy baryons.

The relativized quark model, developed first by Godfrey, Capstick and Isgur[72, 73], has been widely used to investigate the properties of the mesons, baryons, and even the tetraquark states[74–76]. In this model, the relativistic effects are involved, which may be essential for doubly heavy baryon involving a light quark. Since the baryon is a three-body system, its theory is much more complicated compared to the two-body meson system, especially in the calculations of the matrix elements of the Hamiltonian in quark model. In our previous work, we employed a method of infinitesimally-shifted Gaussian(ISG) basis function in the relativized quark model[77, 78], where the calculation of the matrix element is simplified and the baryon is treated as a real three-body system.

In the present work, we use the method in Refs.[77, 78] to study the mass spectra and r.m.s. radii of the excited doubly charmed baryons up to rather high orbital and radial excitations. With the predicted mass spectra, we construct the Regge trajectories in the (J, M^2) planes and determine their Regge slopes and intercepts. Using the wave functions obtained from the relativized quark model, we also study the radial density distributions of the doubly charmed baryons. The paper is organized as follows. After the introduction, we briefly describe the phenomenological methods adopted in this work in Sec.II. In Sec.III we present our numerical results and discussions about Ξ_{cc} and Ω_{cc} . In Sec.IV the baryon Regge trajectories in the (J, M^2) plane are constructed. And Sec V is reserved for our conclusions.

2. PHENOMENOLOGICAL METHODS ADOPTED IN THIS WORK

2.1. Wave function of doubly charmed baryon

The doubly charmed baryon is a three-body system which contains two charmed quarks and one light quark(u , d or s quark) inside. The inter-quark interaction in this three-body system is commonly described by the three sets of Jacobi co-

*Electronic address: yuguoliang2011@163.com

†Electronic address: zhenyuli@163.com

‡Electronic address: zgwang@aliyun.com

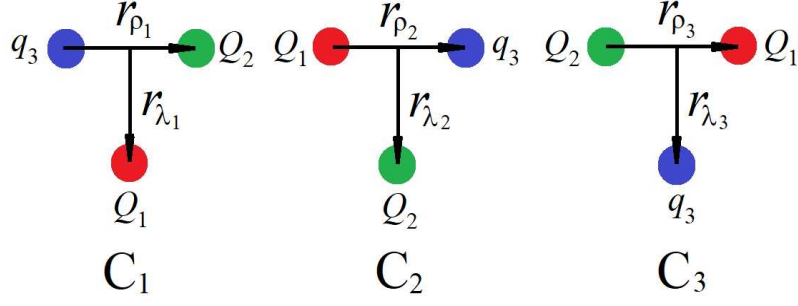


FIG. 1: Jacobi coordinates for the three-body system.

ordinates in Fig. 1. Each set of Jacobi coordinate is called a channel(c) and is defined as,

$$\mathbf{r}_{\lambda_i} = \mathbf{r}_i - \frac{m_j \mathbf{r}_j + m_k \mathbf{r}_k}{m_j + m_k} \quad (1)$$

$$\mathbf{r}_{\rho_i} = \mathbf{r}_j - \mathbf{r}_k \quad (2)$$

where $i, j, k=1, 2, 3$ (or replace their positions in turn). \mathbf{r}_i and m_i denote the position vector and the mass of the i th quark, respectively.

In the heavy quark limit, one light quark within the doubly charmed baryon is decoupled from two heavy quarks. It can be seen from Fig. 1 that channel 3 properly reflects the characteristic of the heavy quark symmetry. Thus, the calculations in this work are performed based on channel 3. Using the transformation of Jacobi coordinates, we can calculate all the matrix elements in channel 3. Under this picture, the degree of freedom between two heavy quarks is commonly called the ρ -mode, while the degree between the center of mass of two heavy quarks and the light quark is called the λ -mode. It was indicated by Refs.[29, 77, 78] that the lowest state of a single heavy baryon is dominated by the λ -mode. We will see in the following analysis that the doubly charmed baryons are dominated by ρ -mode.

In this work, we employ Gaussian basis functions[79] to construct the orbital part of the wave function for a three-body system, which can be written as,

$$\phi_{nlm_l}(\mathbf{r}) = N_{nl} r^l e^{-v_n r^2} Y_{lm_l}(\hat{\mathbf{r}}), \quad (n = 1 - n_{max}) \quad (3)$$

with

$$N_{nl} = \sqrt{\frac{2^{l+2} (2v_n)^{l+3/2}}{\sqrt{\pi} (2l+1)!!}} \quad (4)$$

$$v_n = \frac{1}{r_n^2}, \quad r_n = r_a \left[\frac{r_{amax}}{r_a} \right]^{\frac{n-1}{n_{max}-1}} \quad (5)$$

In Eq.(5), n_{max} is the maximum number of the Gaussian basis functions, r_a and r_{amax} are the Gaussian range parameters. In different studies, people employed different values for r_a and r_{amax} such as $r_a=0.05\sim 0.3$ fm and $r_{amax}=10\sim 15$ fm in Ref.[80], and $r_a=0.1$ fm and $r_{amax}=20$ fm in Ref.[81]. The three parameters n_{max} , r_a and r_{amax} are actually related to each

other. As illustrated in Figs. 2 and 3 in Sec. 3.1, the results show well stability when the parameters are taken as $r_a=0.18$ fm, $r_{amax}=15$ fm with $n_{max} = 9 \sim 12$. The orbital wave function is constructed from the wave functions of the two Jacobi coordinates ρ and λ , and takes the form,

$$\Phi_{l_\rho, l_\lambda, L} = [\phi_{n_\rho, l_\rho, m_\rho}(\mathbf{r}_\rho) \phi_{n_\lambda, l_\lambda, m_\lambda}(\mathbf{r}_\lambda)]_L \quad (6)$$

The spatial part of the wave function includes the spin wave function and orbital part, which can be written as,

$$\psi_{JM} = [[[\chi_{1/2}(Q)\chi_{1/2}(Q)]_s \Phi_{l_\rho, l_\lambda, L}]_j \chi_{1/2}(q)]_{JM} \quad (7)$$

where $\chi_{1/2}$ is the spin wave function of quark and s is the total spin of two heavy quarks. In the heavy quark limit, the coupling scheme of the spin and angular momenta is as, $L = l_\rho + l_\lambda$, $j = s + L$ and $J = j + \frac{1}{2}$. Finally, the full wave function for a definite state of a baryon can be expressed as,

$$\Psi_{full}^{JM} = \sum_{n_\rho, n_\lambda} C_{n_\rho, n_\lambda} \Psi_{JM}(\mathbf{r}_\rho, \mathbf{r}_\lambda) \quad (n_\rho, n_\lambda = 1, \dots, n_{max}) \quad (8)$$

where $\Psi_{JM}(\mathbf{r}_\rho, \mathbf{r}_\lambda)$ is the direct product of color wave function, flavor wave function and the spatial wave function

$$\Psi_{JM}(\mathbf{r}_\rho, \mathbf{r}_\lambda) = \phi_{color} \otimes \phi_{flavor} \otimes \psi_{JM} \quad (9)$$

The state of a doubly charmed baryon can be characterized by a given quantum numbers $l_\rho, l_\lambda, L, s, j$ and J^P .

The flavor wave function and color function of a doubly charmed baryon is symmetric and antisymmetric, respectively. We know that the total wave function must be antisymmetric, thus the spatial part should always be symmetric. For a double quark system in a baryon, its spin wave function is antisymmetric singlet($s = 0$) or symmetric triplet($s = 1$). Correspondingly, the orbital part must also be antisymmetric or symmetric to couple a symmetric spatial wave function. Thus, the total spin s of two charmed quarks(cc) and orbital quantum number l_ρ should satisfy the condition $(-1)^{s+l_\rho} = -1$.

2.2. The relativistic quark model and ISG method

In the relativistic quark model, baryons are formed by three valence(constituent) quarks. They are confined by a confining

potential and interact with each other by residual two-body interactions. In the framework of relativistic quark model, the Hamiltonian for a three-body system is of the form[72, 73],

$$\widehat{H} = \sum_{i=1}^3 (p_i^2 + m_i^2)^{1/2} + \sum_{i<j} \widetilde{H}_{ij}^{\text{conf}} + \sum_{i<j} \widetilde{H}_{ij}^{\text{hyp}} + \sum_{i<j} \widetilde{H}_{ij}^{\text{so}} \quad (10)$$

where the first term is the relativistic kinetic energy term, $\widetilde{H}_{ij}^{\text{conf}}$ is the spin-independent potential including a linear confining potential $\widetilde{S}(r_{ij})$ and the one-gluon exchange potential $G'(r_{ij})$,

$$\widetilde{H}_{ij}^{\text{conf}} = \widetilde{S}(r_{ij}) + G'(r_{ij}) \quad (11)$$

The linear confining potential $\widetilde{S}(r_{ij})$ can be written as,

$$\begin{aligned} \widetilde{S}(r_{ij}) = & -\frac{3}{4} \mathbf{F}_i \cdot \mathbf{F}_j \left\{ br_{ij} \left[\frac{e^{-\sigma_{ij}^2 r_{ij}^2}}{\sqrt{\pi} \sigma_{ij} r_{ij}} \right. \right. \\ & \left. \left. + \left(1 + \frac{1}{2\sigma_{ij}^2 r_{ij}^2}\right) \frac{2}{\sqrt{\pi}} \int_0^{\sigma_{ij} r_{ij}} e^{-x^2} dx \right] + c \right\} \end{aligned} \quad (12)$$

with

$$\sigma_{ij} = \sqrt{s^2 \left[\frac{2m_i m_j}{m_i + m_j} \right]^2 + \sigma_0^2 \left[\frac{1}{2} \left(\frac{4m_i m_j}{(m_i + m_j)^2} \right)^4 + \frac{1}{2} \right]} \quad (13)$$

In Eq.(12), $\mathbf{F}_i \cdot \mathbf{F}_j$ stands for the color matrix and F_n reads,

$$F_n = \begin{cases} \frac{\lambda_n}{2} & \text{for quarks,} \\ -\frac{\lambda_n}{2} & \text{for antiquarks} \end{cases} \quad (14)$$

with $n = 1, 2 \dots 8$. The one-gluon exchange potential $G'(r_{ij})$ can be expressed in terms of one-gluon-exchange propagator $\widetilde{G}(r_{ij})$,

$$G'(r_{ij}) = \left(1 + \frac{p_{ij}^2}{E_i E_j}\right)^{\frac{1}{2}} \widetilde{G}(r_{ij}) \left(1 + \frac{p_{ij}^2}{E_i E_j}\right)^{\frac{1}{2}} \quad (15)$$

with

$$\widetilde{G}(r_{ij}) = \mathbf{F}_i \cdot \mathbf{F}_j \sum_{k=1}^3 \frac{2\alpha_k}{3\sqrt{\pi} r_{ij}} \int_0^{\tau_k r_{ij}} e^{-x^2} dx \quad (16)$$

and $\tau_k = \frac{1}{\sqrt{\frac{1}{\sigma_{ij}^2} + \frac{1}{\nu_k^2}}}$.

In Eq.(10), $\widetilde{H}^{\text{hyp}}$ is the color-hyperfine interaction which contains a tensor interaction and a contact interaction,

$$\widetilde{H}_{ij}^{\text{hyp}} = \widetilde{H}_{ij}^{\text{tensor}} + \widetilde{H}_{ij}^{\text{c}} \quad (17)$$

with

$$\begin{aligned} \widetilde{H}_{ij}^{\text{tensor}} = & -\left(\frac{\mathbf{S}_i \cdot \mathbf{r}_{ij} \mathbf{S}_j \cdot \mathbf{r}_{ij} / r_{ij}^2 - \frac{1}{3} \mathbf{S}_i \cdot \mathbf{S}_j}{m_i m_j} \right) \\ & \times \left(\frac{\partial^2}{\partial r_{ij}^2} - \frac{1}{r_{ij}} \frac{\partial}{\partial r_{ij}} \right) \widetilde{G}_{ij}^{\text{t}}, \end{aligned} \quad (18)$$

$$\widetilde{H}_{ij}^{\text{c}} = \frac{2\mathbf{S}_i \cdot \mathbf{S}_j}{3m_i m_j} \nabla^2 \widetilde{G}_{ij}^{\text{c}} \quad (19)$$

For the spin-orbit interaction, it can also be divided into two parts,

$$\widetilde{H}_{ij}^{\text{so}} = \widetilde{H}_{ij}^{\text{so(v)}} + \widetilde{H}_{ij}^{\text{so(s)}}, \quad (20)$$

with

$$\begin{aligned} \widetilde{H}_{ij}^{\text{so(v)}} = & \frac{\mathbf{S}_i \cdot \mathbf{L}_{ij}}{2m_i^2 r_{ij}} \frac{\partial \widetilde{G}_{ii}^{\text{so(v)}}}{\partial r_{ij}} + \frac{\mathbf{S}_j \cdot \mathbf{L}_{ij}}{2m_j^2 r_{ij}} \frac{\partial \widetilde{G}_{jj}^{\text{so(v)}}}{\partial r_{ij}} \\ & + \frac{(\mathbf{S}_i + \mathbf{S}_j) \cdot \mathbf{L}_{ij}}{m_i m_j r_{ij}} \frac{1}{r_{ij}} \frac{\partial \widetilde{G}_{ij}^{\text{so(v)}}}{\partial r_{ij}} \end{aligned} \quad (21)$$

and

$$\widetilde{H}_{ij}^{\text{so(s)}} = -\frac{\mathbf{S}_i \cdot \mathbf{L}_{ij}}{2m_i^2 r_{ij}} \frac{\partial \widetilde{S}_{ii}^{\text{so(s)}}}{\partial r_{ij}} - \frac{\mathbf{S}_j \cdot \mathbf{L}_{ij}}{2m_j^2 r_{ij}} \frac{\partial \widetilde{S}_{jj}^{\text{so(s)}}}{\partial r_{ij}} \quad (22)$$

In Eqs.(18),(19),(21) and (22), $\widetilde{G}_{ij}^{\text{t}}$, $\widetilde{G}_{ij}^{\text{c}}$, $\widetilde{G}_{ij}^{\text{so(v)}}$ and $\widetilde{S}_{ii}^{\text{so(s)}}$ are achieved from $\widetilde{G}(r_{ij})$ and $\widetilde{S}(r_{ij})$ by introducing momentum-dependent factors,

$$\widetilde{G}_{ij}^{\text{t}} = \left(\frac{m_i m_j}{E_i E_j} \right)^{\frac{1}{2} + \epsilon_1} \widetilde{G}(r_{ij}) \left(\frac{m_i m_j}{E_i E_j} \right)^{\frac{1}{2} + \epsilon_1} \quad (23)$$

$$\widetilde{G}_{ij}^{\text{c}} = \left(\frac{m_i m_j}{E_i E_j} \right)^{\frac{1}{2} + \epsilon_c} \widetilde{G}(r_{ij}) \left(\frac{m_i m_j}{E_i E_j} \right)^{\frac{1}{2} + \epsilon_c} \quad (24)$$

$$\widetilde{G}_{ij}^{\text{so(v)}} = \left(\frac{m_i m_j}{E_i E_j} \right)^{\frac{1}{2} + \epsilon_{\text{so(v)}}} \widetilde{G}(r_{ij}) \left(\frac{m_i m_j}{E_i E_j} \right)^{\frac{1}{2} + \epsilon_{\text{so(v)}}} \quad (25)$$

$$\widetilde{S}_{ii}^{\text{so(s)}} = \left(\frac{m_i^2}{E_i^2} \right)^{\frac{1}{2} + \epsilon_{\text{so(s)}}} \widetilde{S}(r_{ij}) \left(\frac{m_i^2}{E_i^2} \right)^{\frac{1}{2} + \epsilon_{\text{so(s)}}} \quad (26)$$

with $E_i = \sqrt{m_i^2 + p_{ij}^2}$, and ϵ_1 , ϵ_c , $\epsilon_{\text{so(v)}}$ and $\epsilon_{\text{so(s)}}$ are free parameters which take the same values with those in Ref.[77]. The p_{ij} is the magnitude of the momentum of either of the quarks in the ij center-of-mass frame.

For a three-body system, the calculations of the Hamiltonian matrix elements become laborious even with Gaussian basis functions. This process can be simplified by introducing the ISG basis functions. The Gaussian basis function of Eq. (3) is then substituted by the following ISG basis functions[29],

$$\phi_{nlm_l}(\mathbf{r}) = N_{nl} \lim_{\varepsilon \rightarrow 0} \frac{1}{(\nu_n \varepsilon)^l} \sum_{k=1}^{k_{\text{max}}} C_{lm_l, k} e^{-\nu_n (\mathbf{r} - \varepsilon \mathbf{D}_{lm_l, k})^2} \quad (27)$$

where ε is the shifted distance of the Gaussian basis. Taking the limit $\varepsilon \rightarrow 0$ is to be carried out after the matrix elements have been calculated analytically. The coefficient $C_{lm_l, k}$ and the shift-direction vector $\mathbf{D}_{lm_l, k}$ in Eq. (27) are dimensionless

numbers independent of v_n and ε , and they can be described as,

$$C_{lm_i,k} \equiv \sum_{j=0}^{\lfloor \frac{l-m_i}{2} \rfloor} A_{lm_i,j} \sum_{s=0}^p \sum_{t=0}^q \sum_{u=0}^j (-1)^{l-u-t-s} \binom{p}{s} \binom{q}{t} \binom{j}{u} \quad (28)$$

where $p = l - m_l - 2j$, $q = j + m_l$ and

$$\mathbf{D}_{lm_i,k} \equiv \frac{1}{l} [(2s-p)\mathbf{a}_z + (2t-q)\mathbf{a}_{xy} + (2u-j)\mathbf{a}_{xy}^*] \quad (29)$$

with

$$A_{lm_i,j} = \left[\frac{(2l+1)(l-m_i)!}{4\pi(l+m_i)!} \right]^{\frac{1}{2}} \frac{(l+m_i)!(-1)^j}{(-2)^{m_i} 4^j j!(m_l+j)!(l-m_l-2j)!} \quad (30)$$

In relation (29), \mathbf{a}_z , \mathbf{a}_{xy} and \mathbf{a}_{xy}^* are called the shift vectors that are defined as $\mathbf{a}_z \equiv (0, 0, 1)$, $\mathbf{a}_{xy} \equiv (1, i, 0)$, $\mathbf{a}_{xy}^* \equiv (1, -i, 0)$. The spherical harmonic in Eq. (3) is substituted by a sets of coefficients $C_{lm_i,k}$ and vectors $\mathbf{D}_{lm_i,k}$. Thus, the tedious angular momentum algebra and angle integration are avoided, which makes the matrix element calculation easy in practice. For more details about the calculations of the Hamiltonian matrix elements, one can consults our previous work[77].

After all of the matrix elements are evaluated, the mass spectra can be obtained by solving the generalized eigenvalue problem,

$$\sum_{j=1}^{n_{max}^2} (H_{ij} - EN_{ij})C_j = 0, \quad (i = 1 - n_{max}^2) \quad (31)$$

Here, H_{ij} denotes the matrix element in the total color-flavor-spin-spatial base, E is the eigenvalue, C_j stands for the corresponding eigenvector, and N_{ij} is the overlap matrix elements of the Gaussian functions, which arises from the nonorthogonality of the bases and can be expressed as,

$$\begin{aligned} N_{ij} &\equiv \langle \phi_{n_{\rho a} l_{\rho a} m_{\rho a}} | \phi_{n_{\rho b} l_{\rho b} m_{\rho b}} \rangle \times \langle \phi_{n_{\lambda a} l_{\lambda a} m_{\lambda a}} | \phi_{n_{\lambda b} l_{\lambda b} m_{\lambda b}} \rangle \\ &= \left(\frac{2\sqrt{v_{n_{\rho a}} v_{n_{\rho b}}}}{v_{n_{\rho a}} + v_{n_{\rho b}}} \right)^{l_{\rho a} + 3/2} \times \left(\frac{2\sqrt{v_{n_{\lambda a}} v_{n_{\lambda b}}}}{v_{n_{\lambda a}} + v_{n_{\lambda b}}} \right)^{l_{\lambda a} + 3/2} \end{aligned} \quad (32)$$

3. NUMERICAL RESULTS AND DISCUSSIONS

3.1. Numerical stabilities and ρ -modes

The parameters used in the Hamiltonian in Eq.(10) are the same as those in our previous work[77, 78] where the experimental masses of single heavy baryons were well reproduced. In order to investigate the convergence and stability of the numerical results, we plot the masses of the lowest lying $\Xi_{cc}(\frac{1}{2}^+)$ and $\Omega_{cc}(\frac{1}{2}^+)$ baryons in Fig. 2 and the r.m.s. radii $\sqrt{\langle r_{\rho}^2 \rangle}$ and $\sqrt{\langle r_{\lambda}^2 \rangle}$ of the lowest $\Xi_{cc}(\frac{1}{2}^+)$ in Fig. 3. We can see that the results decrease with the basis number and converge to a stable value when the $n_{max}^2 = 100$. Thus, it is reliable for us to carry

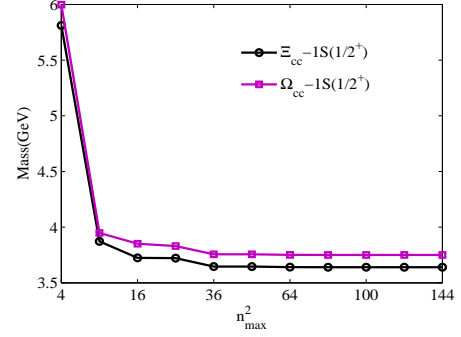


FIG. 2: Convergence of the energy of the lowest Ξ_{cc} and Ω_{cc} for increasing the number of bases functions.

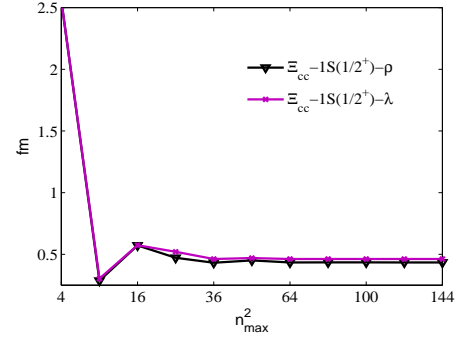


FIG. 3: Convergence of the r.m.s. radius $\sqrt{\langle r_{\rho}^2 \rangle}$ and $\sqrt{\langle r_{\lambda}^2 \rangle}$ of the lowest Ξ_{cc} for increasing the number of bases functions.

out the calculations with 100 Gaussian bases in present work.

For the orbital excitations of doubly charmed baryons, they can be classified by the orbital angular momentum l_{ρ} and l_{λ} . For example, there are two orbital excitation modes λ - and ρ -mode with $(l_{\rho}, l_{\lambda}) = (0, 1)$ and $(1, 0)$ for P -wave baryons. While there are three excitation modes for D -wave baryons with $(l_{\rho}, l_{\lambda}) = (0, 2)$, $(2, 0)$ and $(1, 1)$, which are called the λ -mode, ρ -mode and λ - ρ mixing mode, respectively. For higher orbital

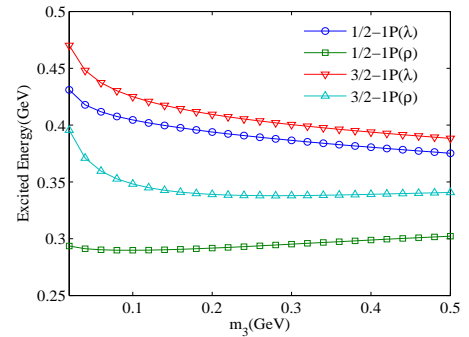


FIG. 4: Quark mass dependence of excited energy of doubly charmed baryons $(\frac{1}{2}^-, \frac{3}{2}^-)$ with λ -mode and ρ -mode

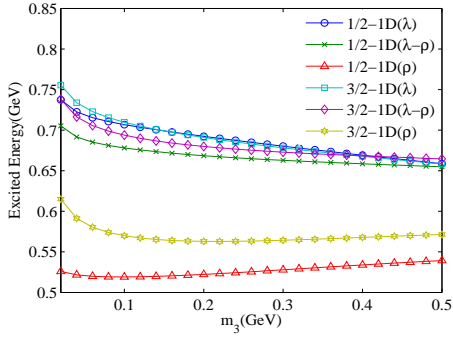


FIG. 5: Quark mass dependence of excited energy of doubly charmed baryons($\frac{1}{2}^+, \frac{3}{2}^+$) with λ -mode, ρ -mode and λ - ρ mixing mode

excited states, their situations are similar to D -wave baryons which also have three excitation modes. By changing the mass of light quark(denoted as m_3 in Figs. 4-5) from 0.01 ~ 0.5 GeV, we plot the excited energy of different excited modes in Figs. 4-5. It is shown that the ρ -mode appears lower in excited energy than both the λ -mode and λ - ρ mixing mode. This indicates the lowest states of doubly charmed baryons are dominated by the ρ -mode whether for P - or D -wave baryons. And this result is consistent with that of Ref.[29].

This above phenomenon originates from the interactions which are dependent on the orbital angular momentum(see Eqs. (21) and (22)). In these interactions, the energy is inversely proportional to the quark masses. Thus, the heavier the mass of quark, the lower the excited energy will be. For the doubly charmed baryons, the ρ -mode excitation between two charmed quarks is lower than the other two excited modes. The situation is just opposite for single heavy baryons that the λ -mode excitation between the center of mass of two light quarks and the heavy quark is the lowest. In the SU(3) limit in the light quark sector, these three orbitally excited modes will mix with each other.

3.2. Mass spectra of Ξ_{cc} and Ω_{cc}

For Ξ_{cc} and Ω_{cc} baryons with ρ excited mode, we obtain their r.m.s. radii and complete mass spectra with quantum numbers up to $n = 4$ and $L = 4$. Many collaborations have focused on the ground state masses of doubly charmed baryons, which results are listed in Table I together with ours. From Table I, we can see that our predicted mass for the ground state of Ξ_{cc} is 3640 MeV. Considering the model uncertainties, this result is consistent with the experimental data 3621.40 MeV. In addition, our predictions for $\Xi_{cc}(\frac{1}{2}^+, \frac{3}{2}^+)$ and $\Omega_{cc}(\frac{1}{2}^+, \frac{3}{2}^+)$ are close to the results from Refs.[14, 22, 23, 44, 50, 60, 68].

For higher radial and orbital excitations together with the ground states, the predicted masses and the r.m.s. radii are shown in Tables III-IV of Appendix A, where each state is characterized by the quantum numbers ($l_\rho l_\lambda L s j$) and $nL(J^P)$ in the first two columns. In order to see the feature of the mass spectra obviously, we show some of the results in Figs. 6-7.

TABLE I: Masses(in MeV) for the ground states of Ξ_{cc} and Ω_{cc} heavy baryons

Baryons	$\Xi_{cc}(\frac{1}{2}^+)$	$\Xi_{cc}^*(\frac{3}{2}^+)$	$\Omega_{cc}(\frac{1}{2}^+)$	$\Omega_{cc}^*(\frac{3}{2}^+)$
Present work	3640	3695	3750	3799
[11]	3676	3753	3815	3876
[14]	3620	3727	3778	3872
[13]	3478	3610	-	-
[48]	3520	3630	3619	3721
[24]	3510	3548	3719	3746
[70]	3676	3746	3787	3851
[23]	3613	3707	3712	3795
[26]	3579	3708	3718	3847
[27]	3678	3752	-	-
[44]	-	3690	-	3780
[28]	3532	3623	3667	3758
[29]	3685	3754	3832	3883
[30]	3606	3675	3715	3772
[22]	3612	3706	3702	3783
[53]	3547	3719	3648	3770
[49]	3557	3661	3710	3800
[31]	3520	3695	3650	3810
[51]	3550	3590	3730	3770
[32]	3679	3763	3830	3891
[67]	3615	3747	-	-
[68]	3627	3690	3692	3756
[60]	3626	3693	3719	3788
[42]	3630	3750	3750	3850
[52]	3620	3620	3720	3720
[69]	3653	3741	-	-
[50]	3604	3714	3726	3820
[33]	3620	3653	3798	3831

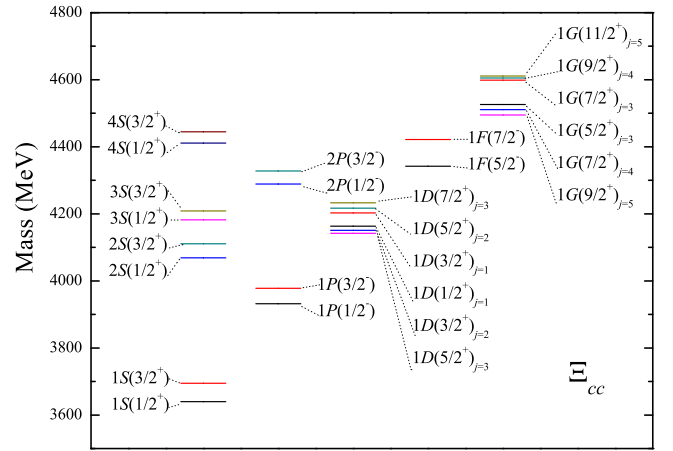


FIG. 6: Mass spectrum of Ξ_{cc} family

From Tables III-IV and Figs. 6-7, we can see that the structure of the mass spectra of Ξ_{cc} and Ω_{cc} are similar to each other. They have the following features: (1) The $1P$ -wave doublet ($\frac{1}{2}^-, \frac{3}{2}^-$) are the lowest excited states, and then is the $2S$ doublet ($\frac{1}{2}^+, \frac{3}{2}^+$). This means they have good potentials to be observed in the future experiments. (2)After considering the spin-orbital interaction, there still exist degeneracy

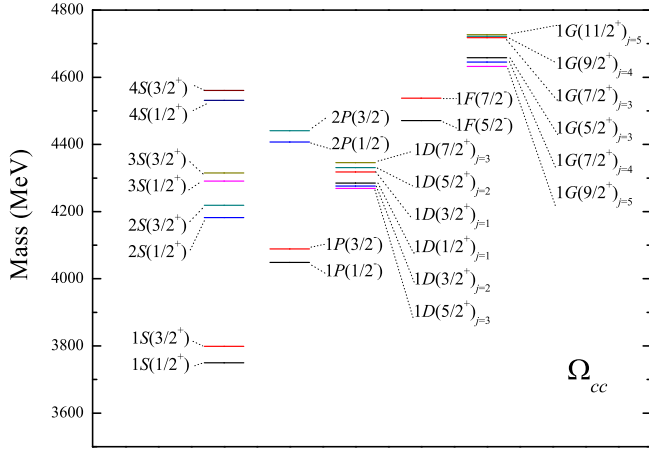


FIG. 7: Mass spectrum of Ω_{cc} family

for higher orbital excited states with different J^P . For example, the excited states $1D(\frac{1}{2}^+)_{j=1}$, $1D(\frac{3}{2}^+)_{j=2}$ and $1D(\frac{5}{2}^+)_{j=3}$ almost lie in the same energy level. (3) For the spin-doublet states, the energy of the $J = j + \frac{1}{2}$ state is higher than that of the $J = j - \frac{1}{2}$ state. (4) The energy difference between two adjacent radial excited states gradually decreases with radial quantum number n increasing.

Because the results of this work cover 1S to 4D states, the open thresholds may occur in this large energy region. Under this circumstance, there are $qqq(q\bar{q})$ configurations possible in baryons, and these must have an effect on the constituent quark model. This coupled effect between bare three-quark state and meson-baryon state or between meson-baryon states can be studied by different methods[82–86]. Some light and single heavy baryons were already studied by considering this coupled-channel effect[82–86]. It was indicated that this coupling has important influence on the light baryons and can significantly suppress the masses of these states[82]. However, its influence on single heavy baryons may be limited[82]. If this coupled-channel effect was also considered in the study of doubly charmed baryons, the masses of these states may also be suppressed, but limited. Nevertheless, its influence on doubly charmed baryons is an interesting problem worth studying and discussing in the future.

3.3. The r.m.s. radii and radial density distributions

The r.m.s. radius and radial density distribution of the baryons are important for testing various conjectures about strongly interacting systems. Thus, using the wave functions obtained from quark model, we also study these parameters. The r.m.s. radii for doubly charmed states are also shown in Tables III-IV, and the radial density distributions are defined

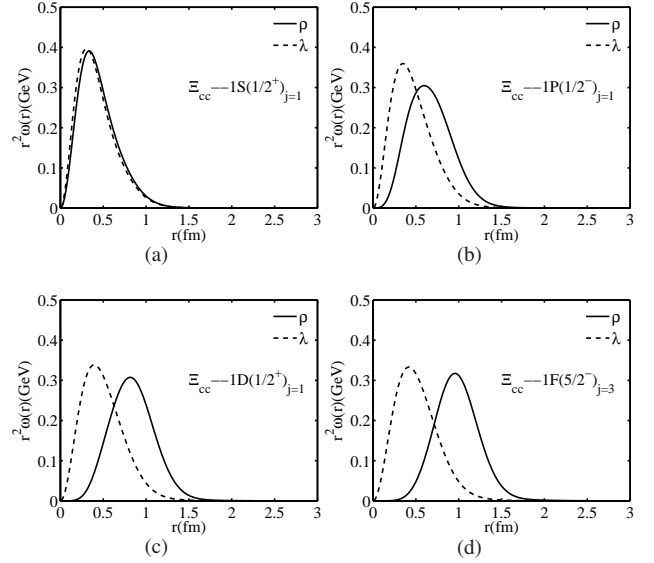


FIG. 8: Radial density distributions for some 1S ~ 1F states in the Ξ_{cc} family

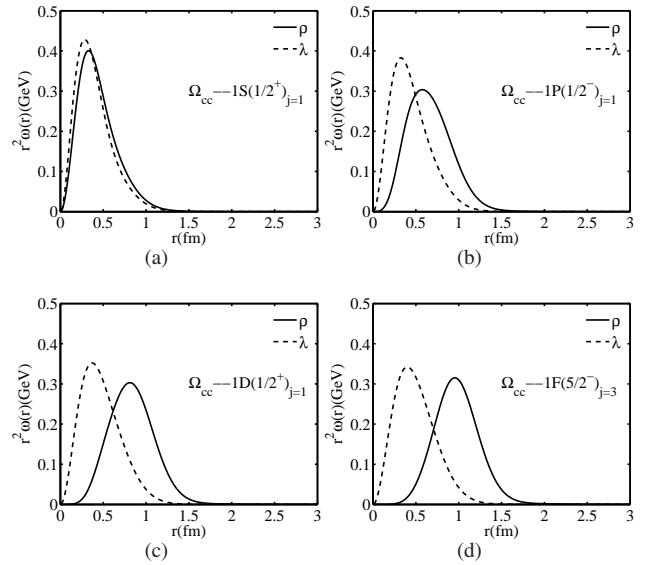


FIG. 9: Radial density distributions for some 1S ~ 1F states in the Ω_{cc} family

as,

$$\begin{aligned} \omega(r_\rho) &= \int |\Psi(\mathbf{r}_\rho, \mathbf{r}_\lambda)|^2 d\mathbf{r}_\lambda d\Omega_\rho \\ \omega(r_\lambda) &= \int |\Psi(\mathbf{r}_\rho, \mathbf{r}_\lambda)|^2 d\mathbf{r}_\rho d\Omega_\lambda \end{aligned} \quad (33)$$

where Ω_ρ and Ω_λ are the solid angles spanned by vectors \mathbf{r}_ρ and \mathbf{r}_λ , respectively. Some of the results about the radial density distributions of baryons Ξ_{cc} and Ω_{cc} are shown in Figs. 8-10.

From Tables III-IV, we can see the r.m.s. radii $\sqrt{\langle r_\rho^2 \rangle}$ and

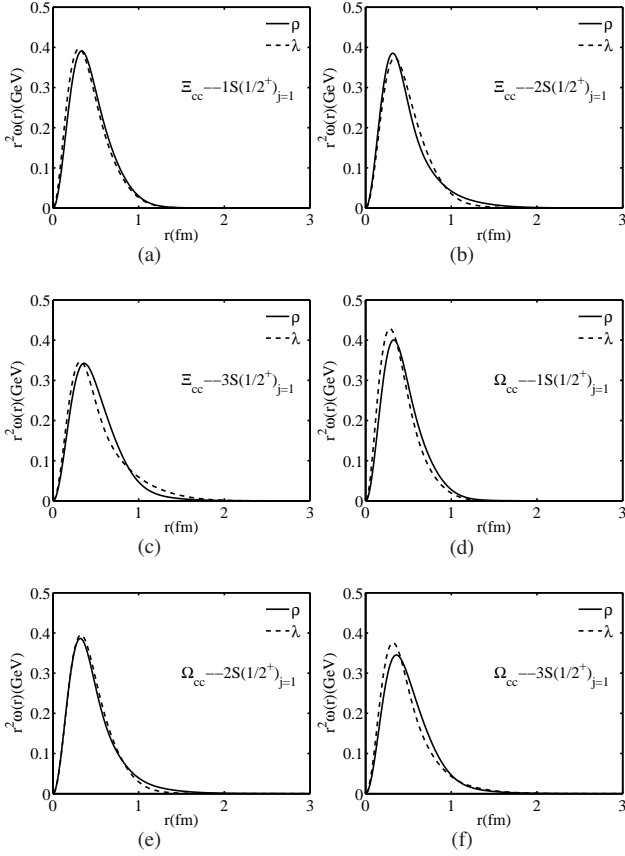


FIG. 10: Radial density distributions for $1S \sim 3S$ states in the Ξ_{cc} family(a-c) and the Ω_{cc} family(d-f).

$\sqrt{\langle r_\lambda^2 \rangle}$ of the $1S(\frac{1}{2}^+)$ state are 0.435 fm, 0.462 fm for Ξ_{cc} , and 0.426 fm, 0.427 fm for Ω_{cc} . In Refs.[87–89], their predicted r.m.s. radii for the ground state of $c\bar{c}$ meson are 0.449 fm, 0.445 fm, and 0.484 fm. These values are comparable with our results for $\sqrt{\langle r_\rho^2 \rangle}$ of doubly charmed baryons. For the states with same radial quantum number n , the $\sqrt{\langle r_\rho^2 \rangle}$ becomes larger obviously when the orbital angular momentum L increases. However, $\sqrt{\langle r_\lambda^2 \rangle}$ increases a little with L increasing. This is consistent with the results shown in Figs. 8-9, where the peak of $r^2\omega(r_\rho)$ shifts outward with L increment and $r^2\omega(r_\lambda)$ changes little. For the states with same angular momentum L , both $\sqrt{\langle r_\rho^2 \rangle}$ and $\sqrt{\langle r_\lambda^2 \rangle}$ increase with radial quantum number n . We can also see this feature from Fig. 10. It is shown that the peak of radial density distribution becomes lower from $1S \sim 3S$ states and the peak position shifts outward slightly. Theoretically, the larger the r.m.s. radii become, the looser the baryons will be. We hope these results can help us to estimate the upper limit of the mass spectra and to search for the new doubly charmed baryons in forthcoming experiments.

From Tables III-IV, we can clearly see another interesting

phenomenon that the order of r.m.s radii $\sqrt{\langle r_\rho^2 \rangle}$ and $\sqrt{\langle r_\lambda^2 \rangle}$ behaves differently with the increment of the radial quantum numbers. For the states from $2D(\frac{1}{2}^+)$ to $4D(\frac{1}{2}^+)$ as examples, their r.m.s radii $\sqrt{\langle r_\rho^2 \rangle}$ and $\sqrt{\langle r_\lambda^2 \rangle}$ alternately increase and decrease, if $\sqrt{\langle r_\rho^2 \rangle}$ increase, $\sqrt{\langle r_\lambda^2 \rangle}$ will decrease. Because all of these D-wave states have definite orbital excitations with $(l_\rho, l_\lambda)=(2,0)$, this phenomenon should be unrelated to orbital excitations. It may be related to the radial excitations, which can be denoted by (n_ρ, n_λ) . The meaning of n_ρ and n_λ in Eq. (6) are similar to l_ρ and l_λ except that the former denotes the radial excitation and the latter is the orbital excitation. The different behaviors of the r.m.s. radii $\sqrt{\langle r_\rho^2 \rangle}$ and $\sqrt{\langle r_\lambda^2 \rangle}$ reflect the distribution of radial excited energy between n_ρ and n_λ . If the radial excited energy of ρ mode is higher than that of λ mode, then $\sqrt{\langle r_\rho^2 \rangle}$ is larger than $\sqrt{\langle r_\lambda^2 \rangle}$. The radial excited energies distribute alternatively between ρ and λ mode with the increment of total radial quantum numbers. Thus, the phenomenon that we see in Tables III-IV emerges.

3.4. Regge trajectories of doubly charmed baryons Ξ_{cc} and Ω_{cc}

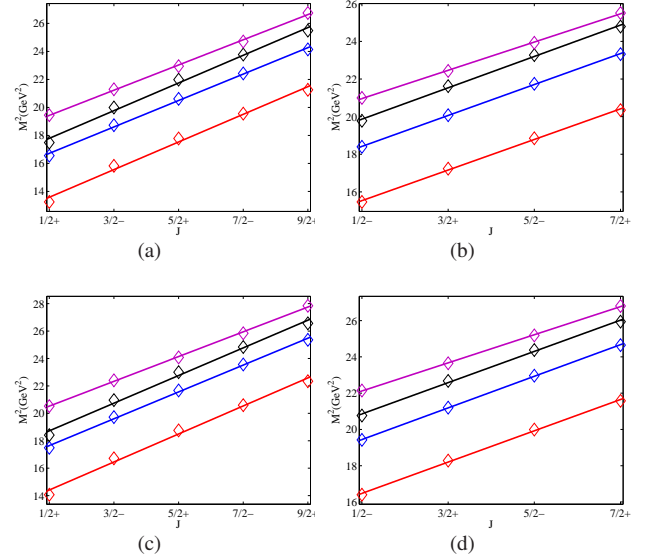


FIG. 11: Parent and daughter Regge trajectories for the Ξ_{cc} baryons with natural parity(a), unnatural parity(b) and Ω_{cc} baryons with natural parity(c), unnatural parity(d)

The Regge theory is very successful in studying the strong interaction at high energy and it is an indispensable tool in phenomenological studies for hadrons[90–99]. In our previous work, we have successfully constructed the Regge trajectories for the single heavy baryons[77, 78]. In the present work, we have obtained the $1S \sim 4S$, $1P \sim 4P$, $1D \sim 4D$, $1F \sim 4F$ and $1G \sim 4G$ state masses for doubly charmed baryons. This makes it easy for us to construct their Regge

trajectories in (J, M^2) plane. The doubly charmed baryons are classified into two groups which have natural parity $S(\frac{1}{2}^+)_{j=1}$, $P(\frac{3}{2}^-)_{j=1}$, $D(\frac{5}{2}^+)_{j=2}$, $F(\frac{7}{2}^-)_{j=3}$, $G(\frac{9}{2}^+)_{j=4}$ and unnatural parity $P(\frac{1}{2}^-)_{j=1}$, $D(\frac{3}{2}^+)_{j=2}$, $F(\frac{5}{2}^-)_{j=3}$, $G(\frac{7}{2}^+)_{j=4}$ [100]. The Regge trajectories are presented in Fig. 11(a)-(b) for Ξ_{cc} and in Fig. 11(c)-(d) for Ω_{cc} , where the predicted masses in quark model are denoted by diamonds. The ground and radial excited states are plotted from bottom to top. We use the following definition about the (J, M^2) Regge trajectories,

$$M^2 = \alpha J + \alpha_0 \quad (34)$$

where α and α_0 are slope and intercept. The straight lines in Fig. 11 are obtained by linear fitting of the predicted values. The fitted slopes and intercepts of the Regge trajectories are listed in Table II. We can see from these figures that all of the predicted masses in our model fit nicely to the linear trajectories in the (J, M^2) plane. These results can help us to assign an accurate position in the mass spectra for observed doubly charmed baryons in the future.

4. CONCLUSIONS

In this work, we have systematically investigate the mass spectra, the r.m.s. radii and the radial density distributions of the doubly charmed baryons Ξ_{cc} , and Ω_{cc} in the frame work of relativized quark model. In addition, with the predicted mass spectra, we also construct the Regge trajectories in (J, M^2) plane. The first feature of this work is that a doubly charmed baryon is regarded as a three-body system of quarks and all quarks contribute fully to the dynamics in the baryon. This is different with the light-quark-heavy-diquark approximation where the three-body problem is reduced to two-body calculations. Second, all parameters in our calculations such as quark masses and parameters of the interquark potential are consistent with those of our previous work[77, 78]. Third, it is the first time that the masses, r.m.s. radii and radial

density distributions of the ground, orbital and radial excited states($1S \sim 4S$, $1P \sim 4P$, $1D \sim 4D$, $1F \sim 4F$ and $1G \sim 4G$) are systematically studied(in Tables III-IV). It is found that model predicted mass of Ξ_{cc}^+ 3640 MeV is in agreement with the experimental data 3621.4 MeV. Finally, for the three orbital excitations λ -mode, ρ -mode and λ - ρ mixing mode, it is shown that the mixing of these excited modes is suppressed and only ρ -mode dominates.

Up to now, only the ground state $1S(\frac{1}{2}^+)$ in Ξ_{cc} family has been observed and confirmed in experiments. The other states that are predicted by quark model in this work, *e.g.* the Ξ_{cc} baryons with quantum numbers $1S(\frac{3}{2}^+)$, $1P(\frac{1}{2}^-)$, $1P(\frac{3}{2}^-)$, and the $1S$ and $1P$ wave Ω_{cc} baryons, are still missing in experiments. These baryons are either the ground state $\Omega_{cc}(\frac{1}{2}^+)$ or the low-lying excitations. They all have good potentials to be observed and need to be searched for by LHCb, BarBar, Bell, CLEO, BESIII collaborations. The ground state $\Omega_{cc}(\frac{1}{2}^+)$ has a mass of 3750 MeV, which is below the threshold of decay channels $\Xi_c D$, $\Xi'_c D$ and $\Xi_{cc} K$, respectively. Thus, it may be searched for in the two-body weak decays[101, 102] $\Omega_{cc} \rightarrow \Omega_c \pi$, $\Omega_{cc} \rightarrow \Xi_c \bar{K}$ and $\Omega_{cc} \rightarrow \Xi'_c \bar{K}$. For the $1S$ wave $\Omega_{cc}(\frac{3}{2}^+)$ and $\Xi_{cc}(\frac{3}{2}^+)$ baryons, their masses are 3799 and 3695 MeV which are also lower than the threshold of their strong decays. The $1P$ wave states of Ξ_{cc} and Ω_{cc} are above the threshold of $\Xi_{cc} \pi$ and $\Xi_{cc} K$, respectively. However, it was studied that these strong decays are forbidden due to the orthogonality of spatial wave functions if the simple harmonic oscillator wave functions were adopted for the $1P$ and $1S$ states[103]. It was suggested that those low-lying doubly charmed baryons have good potentials to be observed in radiative decays[103, 104]. In summary, we hope these analyses can help to search for doubly charmed baryons in future experiments.

Acknowledgments This project is supported by National Natural Science Foundation, Grant Number 12175068 and Natural Science Foundation of HeBei Province, Grant Number A2018502124.

-
- [1] R. L. Workman *et al.* [Particle Data Group], *PTEP* **2022**, 083C01 (2022).
- [2] M. Mattson *et al.* [SELEX], *Phys. Rev. Lett.* **89**, 112001 (2002).
- [3] A. Ocherashvili *et al.* [SELEX], *Phys. Lett. B* **628**, 18-24 (2005).
- [4] S. P. Ratti, *Nucl. Phys. B Proc. Suppl.* **115**, 33-36 (2003).
- [5] B. Aubert *et al.* [BaBar], *Phys. Rev. D* **74**, 011103 (2006).
- [6] R. Chistov *et al.* [Belle], *Phys. Rev. Lett.* **97**, 162001 (2006).
- [7] R. Aaij *et al.* [LHCb], *JHEP* **1312**, 090 (2013).
- [8] R. Aaij *et al.* [LHCb], *Phys. Rev. Lett.* **119**, no.11, 112001 (2017).
- [9] R. Aaij *et al.* [LHCb], *Phys. Rev. Lett.* **121**, no.16, 162002 (2018).
- [10] R. Aaij *et al.* [LHCb], *JHEP* **02**, 049 (2020).
- [11] W. Roberts and M. Pervin, *Int. J. Mod. Phys. A* **23**, 2817-2860 (2008).
- [12] S. Fleck and J. M. Richard, *Prog. Theor. Phys.* **82**, 760-774 (1989).
- [13] S. S. Gershtein, V. V. Kiselev, A. K. Likhoded and A. I. Onishchenko, *Phys. Rev. D* **62**, 054021 (2000).
- [14] D. Ebert, R. N. Faustov, V. O. Galkin and A. P. Martynenko, *Phys. Rev. D* **66**, 014008 (2002).
- [15] A. Majethiya, B. Patel, A. K. Rai and P. C. Vinodkumar, *arXiv:0809.4910 [hep-ph](2008)*.
- [16] A. De Rujula, H. Georgi and S. L. Glashow, *Phys. Rev. D* **12**, 147-162 (1975).
- [17] E. Bagan, H. G. Dosch, P. Gosdzinsky, S. Narison and J. M. Richard, *Z. Phys. C* **64**, 57-72 (1994).
- [18] B. Silvestre-Brac, *Prog. Part. Nucl. Phys.* **36**, 263-273 (1996).
- [19] J. M. Richard, *Nucl. Phys. B Proc. Suppl.* **50**, 147-153 (1996).
- [20] C. Itoh, T. Minamikawa, K. Miura and T. Watanabe, *Phys. Rev. D* **61**, 057502 (2000).
- [21] J. Vijande, H. Garcilazo, A. Valcarce and F. Fernandez, *Phys. Rev. D* **70**, 054022 (2004).
- [22] C. Albertus, E. Hernandez, J. Nieves and J. M. Verde-Velasco,

TABLE II: Fitted parameters α and α_0 for the slope and intercept of the (J, M^2) parent and daughter Regge trajectories for Ξ_{cc} and Ω_{cc} .

Trajectory	$\alpha(\text{GeV}^2)$	$\alpha_0(\text{GeV}^2)$	$\alpha(\text{GeV}^2)$	$\alpha_0(\text{GeV}^2)$
	$\Xi_{cc}(\frac{1}{2}^+)$		$\Xi_{cc}(\frac{1}{2}^-)$	
parent	1.975±0.312	12.601±1.005	1.627±0.192	14.725±0.431
1 daughter	1.887±0.167	15.780±0.420	1.646±0.076	17.591±0.175
2 daughter	1.977±0.297	16.821±0.912	1.668±0.223	19.036±0.512
3 daughter	1.810±0.117	18.530±0.331	1.502±0.101	20.217±0.223
	$\Omega_{cc}(\frac{1}{2}^+)$		$\Omega_{cc}(\frac{1}{2}^-)$	
parent	2.044±0.331	13.392±0.982	1.725±0.204	15.617±0.469
1 daughter	1.958±0.158	16.669±0.429	1.744±0.068	18.569±0.156
2 daughter	2.017±0.297	17.708±0.850	1.723±0.234	19.992±0.536
3 daughter	1.807±0.994	19.626±0.285	1.551±0.083	21.339±0.192

- Eur. Phys. J. A* **32**, 183-199 (2007).
- [23] C. Albertus, E. Hernandez and J. Nieves, *Phys. Lett. B* **683**, 21-25 (2010).
- [24] A. P. Martynenko, *Phys. Lett. B* **663**, 317-321 (2008).
- [25] S. M. Gerasyuta and D. V. Ivanov, *Nuovo Cim. A* **112**, 261-276 (1999).
- [26] Z. Ghalevoni, A. A. Rajabi and M. Hamzavi, *Acta Phys. Polon. B* **42**, 1849-1860 (2011).
- [27] B. Eakins and W. Roberts, *Int. J. Mod. Phys. A* **27**, 1250039 (2012).
- [28] Z. Ghalevoni, A. A. Rajabi, S. x. Qin and D. H. Rischke, *Mod. Phys. Lett. A* **29**, 1450106 (2014).
- [29] T. Yoshida, E. Hiyama, A. Hosaka, M. Oka and K. Sadato, *Phys. Rev. D* **92**, no.11, 114029 (2015).
- [30] Q. F. Lü, K. L. Wang, L. Y. Xiao and X. H. Zhong, *Phys. Rev. D* **96**, no.11, 114006 (2017).
- [31] K. Parattu, S. Chakraborty and T. Padmanabhan, *Eur. Phys. J. C* **76**, no.3, 129 (2016).
- [32] Z. Ghalevoni and M. M. Sorkhi, *Chin. Phys. C* **47**, no.3, 033105 (2023).
- [33] Z. Ghalevoni, C. P. Shen and M. Moazzen Sorkhi, *Phys. Lett. B* **834**, 137405 (2022).
- [34] V. E. Lyubovitskij, A. Faessler, T. Gutsche, M. A. Ivanov and J. G. Korner, *Prog. Part. Nucl. Phys.* **50**, 329-339 (2003).
- [35] L. Tang, X. H. Yuan, C. F. Qiao and X. Q. Li, *Commun. Theor. Phys.* **57**, 435-444 (2012).
- [36] A. K. Likhoded, *Phys. Atom. Nucl.* **72**, 529-535 (2009).
- [37] I. M. Narodetskii, A. N. Plekhanov and A. I. Veselov, *JETP Lett.* **77**, 58-62 (2003).
- [38] H. Mutuk, *Eur. Phys. J. Plus* **137**, no.1, 10 (2022).
- [39] J. R. Zhang and M. Q. Huang, *Phys. Rev. D* **78**, 094007 (2008).
- [40] L. Tang, X. H. Yuan, C. F. Qiao and X. Q. Li, *Commun. Theor. Phys.* **57**, 435-444 (2012).
- [41] Z. G. Wang, *Eur. Phys. J. A* **45**, 267-274 (2010); *Eur. Phys. J. A* **47**, 81-88 (2010).
- [42] Z. G. Wang, *Eur. Phys. J. C* **78**, no.10, 826 (2018); *Eur. Phys. J. C* **72**, 2099 (2012); *Eur. Phys. J. C* **72**, 2099 (2012).
- [43] T. M. Aliev, K. Azizi and M. Savci, *Nucl. Phys. A* **895**, 59-70 (2012).
- [44] T. M. Aliev, K. Azizi and M. Savci, *J. Phys. G* **40**, 065003 (2013).
- [45] V. V. Kiselev and A. E. Kovalsky, *Phys. Rev. D* **64**, 014002 (2001).
- [46] S. Narison and R. Albuquerque, *Phys. Lett. B* **694**, 217-225 (2011).
- [47] H. X. Chen, Q. Mao, W. Chen, X. Liu and S. L. Zhu, *Phys. Rev. D* **96**, no.3, 031501 (2017). [erratum: *Phys. Rev. D* **96**, no.11, 119902 (2017)]
- [48] D. H. He, K. Qian, Y. B. Ding, X. Q. Li and P. N. Shen, *Phys. Rev. D* **70**, 094004 (2004).
- [49] A. Bernotas and V. Simonis, *Lith. J. Phys.* **49**, 19-28 (2009).
- [50] W. X. Zhang, H. Xu and D. Jia, *Phys. Rev. D* **104**, no.11, 114011 (2021).
- [51] D. H. He, K. Qian, Y. B. Ding, X. Q. Li and P. N. Shen, *Phys. Rev. D* **70**, 094004 (2004).
- [52] Q. X. Yu and X. H. Guo, *Nucl. Phys. B* **947**, 114727 (2019).
- [53] F. Giannuzzi, *Phys. Rev. D* **79**, 094002 (2009).
- [54] S. P. Tong, Y. B. Ding, X. H. Guo, H. Y. Jin, X. Q. Li, P. N. Shen and R. Zhang, *Phys. Rev. D* **62**, 054024 (2000).
- [55] M. H. Weng, X. H. Guo and A. W. Thomas, *Phys. Rev. D* **83**, 056006 (2011).
- [56] N. Brambilla, A. Vairo and T. Rosch, *Phys. Rev. D* **72**, 034021 (2005).
- [57] J. Hu and T. Mehen, *Phys. Rev. D* **73**, 054003 (2006). *Phys. Rev. D* **73**, 054003 (2006)
- [58] S. Fleming and T. Mehen, *Phys. Rev. D* **73**, 034502 (2006).
- [59] T. Mehen and B. C. Tiburzi, *Phys. Rev. D* **74**, 054505 (2006).
- [60] H. Bahtiyar, K. U. Can, G. Erkol, M. Oka and T. T. Takahashi, *Phys. Rev. D* **98**, no.11, 114505 (2018).
- [61] R. Lewis, N. Mathur and R. M. Woloshyn, *Phys. Rev. D* **64**, 094509 (2001).
- [62] J. M. Flynn *et al.* [UKQCD], *JHEP* **07**, 066 (2003).
- [63] H. Na and S. A. Gottlieb, *PoS LATTICE2007*, 124 (2007).
- [64] L. Liu, H. W. Lin, K. Orginos and A. Walker-Loud, *Phys. Rev. D* **81**, 094505 (2010).
- [65] Z. S. Brown, W. Detmold, S. Meinel and K. Orginos, *Phys. Rev. D* **90**, no.9, 094507 (2014).
- [66] M. Padmanath, R. G. Edwards, N. Mathur and M. Peardon, *Phys. Rev. D* **91**, no.9, 094502 (2015).
- [67] V. V. Kiselev, A. V. Berezhnoy and A. K. Likhoded, *Phys. Atom. Nucl.* **81**, no.3, 369-372 (2018).
- [68] M. Karliner and J. L. Rosner, *Phys. Rev. D* **97**, no.9, 094006 (2018).
- [69] J. Soto and J. Tarrús Castellà, *Phys. Rev. D* **104**, 074027 (2021).
- [70] D. B. Lichtenberg, R. Roncaglia and E. Predazzi, *Phys. Rev. D* **53**, 6678-6681 (1996).
- [71] J. Oudichhya, K. Gandhi and A. Kumar Rai, *Phys. Scripta* **97**, no.5, 054001 (2022).
- [72] S. Godfrey and N. Isgur, *Phys. Rev. D* **32**, 189-231 (1985).
- [73] S. Capstick and N. Isgur, *Phys. Rev. D* **34**, no.9, 2809-2835 (1986);

- AIP Conf. Proc. **132**, 267-271 (1985).
- [74] Q. F. Lü, D. Y. Chen and Y. B. Dong, *Eur. Phys. J. C* **80**, no.9, 871 (2020).
- [75] Q. F. Lü, D. Y. Chen, Y. B. Dong and E. Santopinto, *Phys. Rev. D* **104**, no.5, 054026 (2021).
- [76] Q. F. Lü, D. Y. Chen and Y. B. Dong, *Phys. Rev. D* **102**, no.7, 074021 (2020).
- [77] G. L. Yu, Z. Y. Li, Z. G. Wang, J. Lu and M. Yan, *Nucl. Phys. B* **990**, 116183 (2023)[arXiv:2206.08128 [hep-ph]].
- [78] Z. Y. Li, G. L. Yu, Z. G. Wang, J. Z. Gu and J. Lu, arXiv:2207.04167[hep-ph](2022).
- [79] M. Kamimura, *Phys. Rev. A* **38**, 621-624 (1988).
- [80] E. Hiyama, Y. Kino and M. Kamimura, *Prog. Part. Nucl. Phys.* **51**, 223-307 (2003).
- [81] Y. W. Pan, T. W. Wu, M. Z. Liu and L. S. Geng, *Phys. Rev. D* **105**, no.11, 114048 (2022)[arXiv:2204.02295 [hep-ph]].
- [82] D. Morel, [arXiv:nucl-th/0204028 [nucl-th]].
- [83] Q. F. Lü, H. Nagahiro and A. Hosaka, *Phys. Rev. D* **107**, no.1, 014025 (2023)[arXiv:2212.02783 [hep-ph]].
- [84] B. Silvestre-Brac and C. Gignoux, *Phys. Rev. D* **43**, 3699-3708 (1991).
- [85] C. Garcia-Recio, V. K. Magas, T. Mizutani, J. Nieves, A. Ramos, L. L. Salcedo and L. Tolos, *Phys. Rev. D* **79**, 054004 (2009).
- [86] V. R. Debastiani, J. M. Dias, W. H. Liang and E. Oset, *Phys. Rev. D* **97**, no.9, 094035 (2018).
- [87] F. Karsch, M. T. Mehr and H. Satz, *Z. Phys. C* **37**, 617 (1988).
- [88] B. Liu, P. N. Shen and H. C. Chiang, *Phys. Rev. C* **55**, 3021-3025 (1997).
- [89] T. Das, *Electron. J. Theor. Phys.* **35**, 207-214 (2016).
- [90] T. Regge, *Nuovo Cim.* **14**, 951 (1959).
- [91] T. Regge, *Nuovo Cim.* **18**, 947-956 (1960).
- [92] G. F. Chew and S. C. Frautschi, *Phys. Rev. Lett.* **7**, 394-397 (1961).
- [93] G. F. Chew and S. C. Frautschi, *Phys. Rev. Lett.* **8**, 41-44 (1962).
- [94] G. S. Bali, *Phys. Rept.* **343**, 1-136 (2001).
- [95] D. V. Bugg, *Phys. Rept.* **397**, 257-358 (2004).
- [96] E. Klempt and A. Zaitsev, *Phys. Rept.* **454**, 1-202 (2007).
- [97] W. Lucha, F. F. Schoberl and D. Gromes, *Phys. Rept.* **200**, 127-240 (1991).
- [98] Y. Nambu, *Phys. Rev. D* **10**, 4262 (1974).
- [99] Y. Nambu, *Phys. Lett. B* **80**, 372-376 (1979).
- [100] D. Ebert, R. N. Faustov and V. O. Galkin, *Phys. Rev. D* **84**, 014025 (2011).
- [101] T. Gutsche, M. A. Ivanov, J. G. Körner, V. E. Lyubovitskij and Z. Tyulemissov, *Phys. Rev. D* **100**, no.11, 114037 (2019).
- [102] H. Y. Cheng, G. Meng, F. Xu and J. Zou, *Phys. Rev. D* **101**, no.3, 034034 (2020).
- [103] L. Y. Xiao, K. L. Wang, Q. f. Lu, X. H. Zhong and S. L. Zhu, *Phys. Rev. D* **96**, no.9, 094005 (2017).
- [104] H. S. Li, L. Meng, Z. W. Liu and S. L. Zhu, *Phys. Lett. B* **777**, 169-176 (2018).

Appendix A: Masses and r.m.s. radii of the Ξ_{cc} and Ω_{cc} heavy baryons

TABLE III: Masses(in MeV) and r.m.s. radii(in fm) of the Ξ_{cc} heavy baryons

$l_\rho l_\lambda L s j$	$nL(J^P)$	M	$\sqrt{\langle r_\rho^2 \rangle}$	$\sqrt{\langle r_\lambda^2 \rangle}$	$l_\rho l_\lambda L s j$	$nL(J^P)$	M	$\sqrt{\langle r_\rho^2 \rangle}$	$\sqrt{\langle r_\lambda^2 \rangle}$
0 0 0 1 1	$1S(\frac{1}{2}^+)$	3640	0.435	0.462	2 0 2 1 3	$1D(\frac{7}{2}^+)$	4233	0.856	0.596
	$2S(\frac{1}{2}^+)$	4069	0.759	0.585		$2D(\frac{7}{2}^+)$	4556	1.200	0.675
	$3S(\frac{1}{2}^+)$	4182	0.524	0.836		$3D(\frac{7}{2}^+)$	4701	0.932	0.959
	$4S(\frac{1}{2}^+)$	4411	1.147	0.658		$4D(\frac{7}{2}^+)$	4807	1.316	0.712
0 0 0 1 1	$1S(\frac{3}{2}^+)$	3695	0.443	0.496	3 0 3 0 3	$1F(\frac{3}{2}^-)$	4342	0.983	0.550
	$2S(\frac{3}{2}^+)$	4111	0.764	0.623		$2F(\frac{3}{2}^-)$	4663	1.347	0.629
	$3S(\frac{3}{2}^+)$	4209	0.539	0.851		$3F(\frac{3}{2}^-)$	4824	1.097	0.925
	$4S(\frac{3}{2}^+)$	4445	1.147	0.689		$4F(\frac{3}{2}^-)$	4891	1.372	0.661
1 0 1 0 1	$1P(\frac{1}{2}^-)$	3932	0.642	0.502	3 0 3 0 3	$1F(\frac{7}{2}^-)$	4422	1.007	0.625
	$2P(\frac{1}{2}^-)$	4289	0.946	0.589		$2F(\frac{7}{2}^-)$	4736	1.426	0.712
	$3P(\frac{1}{2}^-)$	4447	0.717	0.886		$3F(\frac{7}{2}^-)$	4876	1.093	0.984
	$4P(\frac{1}{2}^-)$	4582	1.299	0.669		$4F(\frac{7}{2}^-)$	4971	1.298	0.711
1 0 1 0 1	$1P(\frac{3}{2}^-)$	3978	0.654	0.536	4 0 4 1 3	$1G(\frac{3}{2}^+)$	4526	1.121	0.577
	$2P(\frac{3}{2}^-)$	4328	0.963	0.622		$2G(\frac{3}{2}^+)$	4843	1.600	0.672
	$3P(\frac{3}{2}^-)$	4472	0.722	0.907		$3G(\frac{3}{2}^+)$	4990	1.233	0.944
	$4P(\frac{3}{2}^-)$	4615	1.290	0.695		$4G(\frac{3}{2}^+)$	5063	1.308	0.652
2 0 2 1 1	$1D(\frac{1}{2}^+)$	4163	0.819	0.538	4 0 4 1 3	$1G(\frac{7}{2}^+)$	4599	1.142	0.650
	$2D(\frac{1}{2}^+)$	4490	1.121	0.614		$2G(\frac{7}{2}^+)$	4905	1.669	0.752
	$3D(\frac{1}{2}^+)$	4656	0.908	0.916		$3G(\frac{7}{2}^+)$	5041	1.224	1.006
	$4D(\frac{1}{2}^+)$	4745	1.381	0.679		$4G(\frac{7}{2}^+)$	5146	1.240	0.705
2 0 2 1 1	$1D(\frac{3}{2}^+)$	4203	0.831	0.572	4 0 4 1 4	$1G(\frac{7}{2}^+)$	4511	1.120	0.565
	$2D(\frac{3}{2}^+)$	4526	1.148	0.648		$2G(\frac{7}{2}^+)$	4829	1.599	0.660
	$3D(\frac{3}{2}^+)$	4679	0.911	0.940		$3G(\frac{7}{2}^+)$	4979	1.236	0.936
	$4D(\frac{3}{2}^+)$	4777	1.359	0.703		$4G(\frac{7}{2}^+)$	5050	1.310	0.642
2 0 2 1 2	$1D(\frac{3}{2}^+)$	4151	0.821	0.528	4 0 4 1 4	$1G(\frac{9}{2}^+)$	4605	1.147	0.659
	$2D(\frac{3}{2}^+)$	4481	1.124	0.604		$2G(\frac{9}{2}^+)$	4909	1.683	0.762
	$3D(\frac{3}{2}^+)$	4650	0.915	0.910		$3G(\frac{9}{2}^+)$	5045	1.225	1.014
	$4D(\frac{3}{2}^+)$	4736	1.379	0.669		$4G(\frac{9}{2}^+)$	5158	1.227	0.713
2 0 2 1 2	$1D(\frac{5}{2}^+)$	4217	0.841	0.583	4 0 4 1 5	$1G(\frac{9}{2}^+)$	4495	1.122	0.553
	$2D(\frac{5}{2}^+)$	4540	1.169	0.660		$2G(\frac{9}{2}^+)$	4816	1.603	0.649
	$3D(\frac{5}{2}^+)$	4689	0.919	0.949		$3G(\frac{9}{2}^+)$	4968	1.238	0.929
	$4D(\frac{5}{2}^+)$	4790	1.342	0.708		$4G(\frac{9}{2}^+)$	5039	1.305	0.630
2 0 2 1 3	$1D(\frac{5}{2}^+)$	4142	0.829	0.519	4 0 4 1 5	$1G(\frac{11}{2}^+)$	4611	1.154	0.669
	$2D(\frac{5}{2}^+)$	4474	1.135	0.594		$2G(\frac{11}{2}^+)$	4914	1.700	0.773
	$3D(\frac{5}{2}^+)$	4647	0.926	0.905		$3G(\frac{11}{2}^+)$	5048	1.228	1.024
	$4D(\frac{5}{2}^+)$	4729	1.371	0.658		$4G(\frac{11}{2}^+)$	5172	1.214	0.722

TABLE IV: Masses(in MeV) and r.m.s. radii(in fm) of the Ω_{cc} heavy baryons

$l_\rho l_\lambda L s j$	$nL(J^P)$	M	$\sqrt{\langle r_\rho^2 \rangle}$	$\sqrt{\langle r_\lambda^2 \rangle}$	$l_\rho l_\lambda L s j$	$nL(J^P)$	M	$\sqrt{\langle r_\rho^2 \rangle}$	$\sqrt{\langle r_\lambda^2 \rangle}$
0 0 0 1 1	$1S(\frac{1}{2}^+)$	3750	0.426	0.427	2 0 2 1 3	$1D(\frac{7}{2}^+)$	4346	0.844	0.553
	$2S(\frac{1}{2}^+)$	4182	0.731	0.567		$2D(\frac{7}{2}^+)$	4671	1.159	0.633
	$3S(\frac{1}{2}^+)$	4291	0.540	0.775		$3D(\frac{7}{2}^+)$	4807	0.932	0.907
	$4S(\frac{1}{2}^+)$	4531	1.120	0.650		$4D(\frac{7}{2}^+)$	4921	1.345	0.682
0 0 0 1 1	$1S(\frac{3}{2}^+)$	3799	0.435	0.457	3 0 3 0 3	$1F(\frac{5}{2}^-)$	4471	0.973	0.519
	$2S(\frac{3}{2}^+)$	4219	0.735	0.599		$2F(\frac{5}{2}^-)$	4792	1.302	0.598
	$3S(\frac{3}{2}^+)$	4315	0.553	0.790		$3F(\frac{5}{2}^-)$	4937	1.094	0.878
	$4S(\frac{3}{2}^+)$	4561	1.121	0.677		$4F(\frac{5}{2}^-)$	5018	1.414	0.636
1 0 1 0 1	$1P(\frac{1}{2}^-)$	4049	0.631	0.468	3 0 3 0 3	$1F(\frac{7}{2}^-)$	4538	0.995	0.582
	$2P(\frac{1}{2}^-)$	4407	0.922	0.561		$2F(\frac{7}{2}^-)$	4854	1.377	0.667
	$3P(\frac{1}{2}^-)$	4557	0.718	0.834		$3F(\frac{7}{2}^-)$	4984	1.098	0.932
	$4P(\frac{1}{2}^-)$	4706	1.298	0.646		$4F(\frac{7}{2}^-)$	5083	1.343	0.681
1 0 1 0 1	$1P(\frac{3}{2}^-)$	4089	0.642	0.497	4 0 4 1 3	$1G(\frac{3}{2}^+)$	4658	1.112	0.545
	$2P(\frac{3}{2}^-)$	4441	0.936	0.589		$2G(\frac{3}{2}^+)$	4976	1.551	0.639
	$3P(\frac{3}{2}^-)$	4579	0.723	0.854		$3G(\frac{3}{2}^+)$	5104	1.242	0.897
	$4P(\frac{3}{2}^-)$	4734	1.292	0.667		$4G(\frac{3}{2}^+)$	5188	1.357	0.629
2 0 2 1 1	$1D(\frac{1}{2}^+)$	4285	0.807	0.504	4 0 4 1 3	$1G(\frac{7}{2}^+)$	4718	1.131	0.607
	$2D(\frac{1}{2}^+)$	4612	1.088	0.582		$2G(\frac{7}{2}^+)$	5028	1.623	0.706
	$3D(\frac{1}{2}^+)$	4767	0.904	0.867		$3G(\frac{7}{2}^+)$	5148	1.238	0.954
	$4D(\frac{1}{2}^+)$	4870	1.402	0.654		$4G(\frac{7}{2}^+)$	5255	1.285	0.677
2 0 2 1 1	$1D(\frac{3}{2}^+)$	4318	0.818	0.532	4 0 4 1 4	$1G(\frac{5}{2}^+)$	4645	1.112	0.536
	$2D(\frac{3}{2}^+)$	4642	1.111	0.610		$2G(\frac{5}{2}^+)$	4965	1.550	0.629
	$3D(\frac{3}{2}^+)$	4788	0.908	0.889		$3G(\frac{5}{2}^+)$	5093	1.244	0.889
	$4D(\frac{3}{2}^+)$	4896	1.384	0.674		$4G(\frac{5}{2}^+)$	5177	1.358	0.620
2 0 2 1 2	$1D(\frac{5}{2}^+)$	4276	0.810	0.496	4 0 4 1 4	$1G(\frac{9}{2}^+)$	4722	1.136	0.615
	$2D(\frac{5}{2}^+)$	4604	1.091	0.573		$2G(\frac{9}{2}^+)$	5032	1.640	0.715
	$3D(\frac{5}{2}^+)$	4762	0.910	0.861		$3G(\frac{9}{2}^+)$	5151	1.239	0.963
	$4D(\frac{5}{2}^+)$	4863	1.400	0.645		$4G(\frac{9}{2}^+)$	5265	1.269	0.684
2 0 2 1 2	$1D(\frac{7}{2}^+)$	4331	0.829	0.543	4 0 4 1 5	$1G(\frac{7}{2}^+)$	4632	1.114	0.526
	$2D(\frac{7}{2}^+)$	4655	1.130	0.620		$2G(\frac{7}{2}^+)$	4954	1.556	0.620
	$3D(\frac{7}{2}^+)$	4796	0.917	0.897		$3G(\frac{7}{2}^+)$	5084	1.247	0.882
	$4D(\frac{7}{2}^+)$	4907	1.369	0.678		$4G(\frac{7}{2}^+)$	5168	1.352	0.609
2 0 2 1 3	$1D(\frac{9}{2}^+)$	4269	0.818	0.488	4 0 4 1 5	$1G(\frac{11}{2}^+)$	4727	1.142	0.622
	$2D(\frac{9}{2}^+)$	4600	1.101	0.566		$2G(\frac{11}{2}^+)$	5036	1.660	0.725
	$3D(\frac{9}{2}^+)$	4759	0.922	0.856		$3G(\frac{11}{2}^+)$	5154	1.242	0.971
	$4D(\frac{9}{2}^+)$	4857	1.392	0.635		$4G(\frac{11}{2}^+)$	5277	1.252	0.692